Original Article

Mitochondrial Autophagy and NLRP3 Inflammasome in Pulmonary Tissues from Severe Combined Immunodeficient Mice after Cardiac Arrest and Cardiopulmonary Resuscitation

Jing-Jun Lyu[1], Jawahar L Mehta[2], Yi Li[3], Lu Ye[1], Sheng-Nan Sun[1], Hong-Shuang Sun[1], Jia-Chang Li[1], Dong-Mei Zhang[1], Jie Wei[1]

[1]Department of Emergency, Renmin Hospital of Wuhan University, Wuhan, Hubei 430060, China
[2]Department of Medicine, Central Arkansas Veterans Healthcare System, University of Arkansas for Medical Sciences, Little Rock, AR 72205, USA
[3]Department of Emergency, Peking Union Medical College Hospital, Beijing 100032, China

Abstract

Background: The incidence of cancer, diabetes, and autoimmune diseases has been increasing. Furthermore, there are more and more patients with solid organ transplants. The survival rate of these immunocompromised individuals is extremely low when they are severely hit-on. In this study, we established cardiac arrest cardiopulmonary resuscitation (CPR) model in severe combined immunodeficient (SCID) mice, analyzed the expression and activation of mitochondrial autophagy and NLRP3 inflammasome/caspase-1, and explored mitochondrial repair and inflammatory injury in immunodeficiency individual during systemic ischemia-reperfusion injury.

Methods: A potassium chloride-induced cardiac arrest model was established in C57BL/6 and nonobese diabetic/SCID (NOD/SCID) mice. One hundred male C57BL/6 mice and 100 male NOD/SCID mice were randomly divided into five groups (control, 2 h post-CPR, 12 h post-CPR, 24 h post-CPR, and 48 h post-CPR). A temporal dynamic view of alveolar epithelial cells, macrophages, and neutrophils from bronchoalveolar lavage fluid (BALF) was obtained using Giemsa staining. Spatial characterization of phenotypic analysis of macrophages in the lung interstitial tissue was analyzed by flow cytometry. The morphological changes of mitochondria 48 h after CPR were studied by transmission electron microscopy and quantified according to the Flameng grading system. Western blotting analysis was used to detect the expression and activation of the markers of mitochondrial autophagy, NLRP3 inflammasome, and caspase-1.

Results: (1) In NOD/SCID mice, macrophages were disintegrated in BALF, and many alveolar epithelial cells were shed at 48 h after resuscitation. Compared with C57BL/6 mice, the ratio of macrophages/total cells peaked at 12 h and was significantly higher in NOD/SCID mice (31.17 ± 4.13 vs. 49.69 ± 2.43, $t = 14.46$, $P = 0.001$). After 24 h, the results showed a downward trend. Furthermore, a large number of macrophages were disintegrated in the BALF. (2) Mitochondrial autophagy was present in both C57BL/6 and NOD/SCID mice after CPR, but it began late in the NOD/SCID mice. Compared with C57BL/6 mice, phos-ULK1 (Ser^{327}) expression was significantly lower at 2 h and 12 h after CPR (2 h after CPR: 1.88 ± 0.36 vs. 1.12 ± 0.11, $t = -1.36$, $P < 0.01$ and 12 h after CPR: 1.52 ± 0.16 vs. 1.05 ± 0.12, $t = -0.33$, $P < 0.01$), whereas phos-ULK1 (Ser^{757}) expression was significantly higher at 2 h and 12 h after CPR in NOD/SCID mice (2 h after CPR: 1.28 ± 0.12 vs. 1.69 ± 0.14, $t = 1.7$, $P < 0.01$ and 12 h after CPR: 1.33 ± 0.10 vs. 1.94 ± 0.13, $t = 2.75$, $P < 0.01$). (3) Furthermore, NLRP3 inflammasome/caspase-1 activation in the pulmonary tissues occurred early and for only a short time in C57BL/6 mice, but this phenomenon was sustained in NOD/SCID mice. The expression of the NLRP3 inflammasome increased modestly in the C57 mice, but the increase was higher in the NOD/SCID mice than in the C57BL/6 mice, especially at 12, 24, 48 h after CPR (48 h after CPR: 1.46 ± 0.13 vs. 2.97 ± 0.19, $t = 5.34$, $P = 0.001$). The expression of caspase-1-20 generally followed the same pattern as the NLRP3 inflammasome.

Conclusions: There is a regulatory relationship between the NLRP3 inflammasome and mitochondrial autophagy after CPR in the healthy mice. This regulatory relationship was disturbed in the NOD/SCID mice because the signals for mitochondrial autophagy occurred late, and NLRP3 inflammasome- and caspase-1-dependent cell injury was sustained.

Key words: Autophagy; Cardiopulmonary Resuscitation; Immunodeficiency; Macrophage; Mitochondria; NLRP3 Inflammasome

Address for correspondence: Dr. Jing-Jun Lyu, Department of Emergency, Renmin Hospital of Wuhan University, Wuhan, Hubei 430060, China
E-Mail: lvjingjun@whu.edu.cn

Access this article online

Quick Response Code:

Website: www.cmj.org

DOI: 10.4103/0366-6999.231519

Received: 29-01-2018 **Edited by:** Li-Shao Guo
How to cite this article: Lyu JJ, Mehta JL, Li Y, Ye L, Sun SN, Sun HS, Li JC, Zhang DM, Wei J. Mitochondrial Autophagy and NLRP3 Inflammasome in Pulmonary Tissues from Severe Combined Immunodeficient Mice after Cardiac Arrest and Cardiopulmonary Resuscitation. Chin Med J 2018;131:1174-84.

Introduction

Cardiac arrest is the leading cause of death in the world. Its incidence is far higher than that of sepsis. Postcardiac arrest syndrome (PCAS) is the pathological process of a systemic ischemia-reperfusion injury (I/R injury) induced by cardiopulmonary resuscitation (CPR) after cardiac arrest. PCAS, which manifests as systemic inflammatory response syndrome, ends in multiple organ dysfunction syndrome, especially in immunosuppressed participants.[1] This phenomenon occurs relatively infrequently in healthy participants who receive CPR. However, the mechanisms underlying multiple organ dysfunction syndrome in immunosuppressed participants have yet to be fully characterized.

Mitochondria are extremely sensitive to I/R injury. Sudden elevation of reactive oxygen species (ROS) induces the mitochondrial permeability transition pore (mPTP) opening and mitochondrial polarization, which determines the fate of the cell.[2-8] Minor injuries lead to decreases in the mitochondrial membrane potential and mPTP opening, which subsequently causes mitochondrial autophagy. Mitochondrial autophagy not only selectively removes impaired mitochondria but also prevents the production of ROS by damaged mitochondria. Mitochondria autophagy ameliorates the inflammatory response.[9-19] However, the mechanism of mitochondrial autophagy in the progressive development of Cardiac Arrest-Systemic Inflammatory Response Syndrome (CA-SIRS) to Cardiac Arrest-Multiple Organ Dysfunction Syndrome (CA-MODS) after cardiac arrest remains unclear.

Clinical studies have shown that the survival rate after CPR in immunocompromised patients is significantly lower than that in individuals with normal immune function. We investigated mitochondrial autophagy and the NLRP3 inflammasome in the pulmonary system of NOD/SCID mice for 48 h after CPR.

Methods

Animal protocol

One hundred healthy adult male C57BL/6 mice of specific pathogen-free grade (weighing 22 ± 2 g, age 56–63 days) and 100 nonobese diabetic/severe combined immuno-deficient (NOD/SCID) adult male mice of surface plasmon resonance grade (weighing 24 ± 2 g, age 56–63 days) were provided by Beijing HuaFukang Bioscience Co., Inc. (Beijing, China), Production License Number: SCXK (Beijing) 2009-0004.

NOD/SCID mice were established in The Jackson Laboratory (Bar Harbor, ME, USA). SCID mice possess an autosomal recessive mutation developed in C.B-17 mice, which are a congenic and inbred strain of BALB mice. SCID mice share a similar genetic background with BALB/c mice. NOD/SCID mice are developed by reciprocal crossing with NOD/Lt mice at the Jackson Laboratory to decrease the natural killer (NK) cell activity. Thus, NOD/SCID mice, also known as immunodeficient mice, lack T lymphocytes and B lymphocytes and exhibit low NK cell activity.

The animals were maintained in the Experimental Animal Center of Renmin Hospital of Wuhan University (license number: S0271402213A). All experimental procedures were performed according to protocols approved by the Institutional Animal Care and Use Committee.

Experimental groups

C57BL/6 (100 mice) and NOD/SCID (100 mice) groups were each randomly divided into the control group (8 mice) and model groups (92 mice). After the return of spontaneous circulation (ROSC), the mice in the model group were further divided into four groups including groups for 2 h after resuscitation, 12 h after resuscitation, 24 h after resuscitation, and 48 h after resuscitation.

Cardiac arrest and cardiopulmonary resuscitation mouse model

Mice were weighed and anesthetized by an intraperitoneal injection of 3% pentobarbital sodium. The trachea was intubated with a 22-gauge catheter, and the mice were subjected to mechanical ventilation (respiratory rate: 100–130/min, tidal volume: 0.2 ml, and inspiratory-expiratory ratio: 1:1). During the surgical procedure, electrocardiogram (ECG) was recorded.

A mouse model of cardiac arrest induced by high potassium chloride was established. After the tracheal tube position was secured and the heart rate (HR) was >300 beats/min, a potassium chloride solution (50 μl and 0.5 mol) at 1.6–2.0 μl/g body weight was injected through the jugular vein to induce immediate cardiac arrest. Then, after the ventilator stopped for 150 s, chest compression was given manually for 3 min. If ROSC failed to appear at 3 min after CPR, resuscitation was discontinued. After CPR and ROSC, HR was continuously monitored, and assisted respiration was performed using a ventilator. After ROSC, the tracheal catheter and the ventilator were removed.

Cardiac arrest was characterized by (1) ventricular fibrillation, electromechanical dissociation, or ventricular standstill as shown by ECG, (2) disappearance of beats in the apical region of the heart, and (3) cyanosis of lips or limbs.

ROSC was determined by (1) normal ECG, (2) HR >200 beats/min, recovered respiration, and physiological reflex, (3) obvious cardiac impulse in the apical region of the heart, and (4) alleviated cyanosis of lips or limbs. Animals undergoing ROSC exhibited abdominal respiration even 5 min after removing the ventilator.

Bronchoalveolar lavage fluid analysis and measurement of cellular reactive oxygen species

The bronchoalveolar lavage fluid (BALF) was collected through an intratracheal cannula with three sequential 1 ml aliquots of 0.9% sterile saline (unclear), and the samples were centrifuged at 1500 rpm/min for 10 min at 4°C. The cell pellet was resuspended in 0.9% sterile saline for differential cell counts including identifying alveolar epithelial cells, macrophages, and neutrophils through Giemsa staining.

Phenotypic analysis of pulmonary interstitial macrophages by flow cytometry

The right lower lobe of lavaged lungs was minced with fine scissors and enzymatically digested with 0.1% Type I collagenase (Sigma-Aldrich, USA) for 1 h at 37°C with gentle agitation every 20 min. The single cell suspension was refiltered through a 40 μm nylon mesh after digestion to remove connective tissue and then was washed with D-Hanks. Cell viability was determined with Trypan blue staining.

Phenotypic analysis of pulmonary interstitial macrophages was performed using flow cytometry. The gating strategy for analyzing interstitial macrophages was the same as in previous reports with some modifications.[20-22] In brief, the isolated cells were incubated with PE/Cy5-F4/80, PE-CD206, PE/Cy7-CD11c antibodies, and CD11b antibodies (BioLegend, San Diego, CA, USA) at the concentrations recommended in the manufacturer's protocol [Supplementary Figure 1]. After 15 min of incubation, flow cytometric analysis was performed to detect migrating macrophages ($CD11b^+$ $CD11C^-$), macrophages *in situ* ($CD11b^-$ $CD11C^+$), and macrophage debris ($CD11b^-$ $CD11C^-$). Phenotypic analysis of the pulmonary interstitial macrophages was performed with a Cytomics FC500 Flow Cytometer (Beckman Coulter, USA) and analyzed with FlowJox 10.0.7r2 software (Treestar, Ashland, OR, USA).

Cellular ROS was measured with a DCFDA Cellular ROS Detection Assay Kit (Abcam, Cambridge, MA, USA). Fluorescence of DCFDA was measured on the FL-1 channel with an excitation wavelength of 485 nm and an emission wavelength of 535 nm (FACS Vantage SE, Becton Dickinson, USA).[23] The data were recorded with the use of Flowing Software 2.0 as the "M2 percentage" fluorescence variation, which indicates the percentage of cells with enhanced ROS production.[23]

Mitochondrial morphology and semiquantitative analysis in the lung tissues

Transmission electron microscopy (TEM) specimens were prepared as follows. Each cubic millimeter of fresh pulmonary tissue was fixed with 4% glutaraldehyde followed by osmium tetroxide. After being washed with phosphate-buffered saline, the tissues were dehydrated in an alcohol series. The embedding agent and 100% acetone were added at a 1:1 ratio for 1 h. The tissue pieces were placed into capsules for embedding and placed in an oven. Ultrathin sections were obtained, and lead citrate staining was performed. The resulting sections were subjected to examination for ultrastructure using a transmission electron microscope (H-7700, Hitachi, Japan).

The mitochondrial structure was semi-quantified using TEM and the Flameng grading system. In each animal, 100 mitochondria were randomly selected in five fields (20 mitochondria in each field). The mitochondrial structure was scored from 1 to 4 (the higher the level, the more severe the injury of mitochondrial structure), and the average score for each animal was determined from 100 scores.

The Flameng grading system is as follows: Score 0, intact mitochondria with mitochondrial granules; Score 1, the structure of the mitochondria remains intact, but the mitochondrial granules are absent; Score 2, swollen mitochondria with cleared matrix but intact cristae and membrane; Score 3, severe mitochondrial swelling, broken cristae with matrix clearing but membrane intact; and Score 4, the mitochondrial cristae are broken and the intact mitochondrial membranes disappear.

Western blotting analysis

Mitochondrial autophagy markers and regulatory molecules, i.e., ULK1, beclin-1, LC3-II, and their phosphorylated forms, were measured in the pulmonary tissues by Western blotting. NLRP3 inflammasome, pro-Casp-1, caspase-1p20, and cell apoptosis molecules from the mitochondria were released including Smac/Diablo, cytochrome c (cyto c), and BAX as well as glyceraldehyde-3-phosphate dehydrogenase (GAPDH) or beta-actin, which were also measured by Western blotting.

Primary antibodies were purchased from Cell Signaling Technology (Danvers, MA, USA) or Abcam. The densities of protein bands were quantified using the Odyssey two-color infrared laser imaging system (Millipore, Billerica, MA, USA), and the band intensities were normalized to GAPDH or beta-actin.

Statistical analysis

The data were analyzed using SPSS 20.0 software (SPSS, Chicago, IL, USA). Measurement data verified for normality and homogeneity of variance are presented as the mean ± standard deviation and analyzed by *t*-test. Otherwise, the data are described as the median (25/75 percentiles) and analyzed by the Mann–Whitney *U*-test. The enumeration data were analyzed using the Chi-square test. $P < 0.05$ was considered to indicate statistical significance.

Results

Return of spontaneous circulation and survival rates during 48 h after cardiopulmonary resuscitation

The ROSC rates and survival rates during the 48 h after CPR in C57BL/6 and NOD/SCID mice are shown in Table 1. Compared to C57BL/6 mice, NOD/SCID mice had a higher body weight, even at the same age, and they were resistant to tracheal intubation and intravenous administration. These animals had a higher ROSC rate that was not significantly different. Importantly, the survival rate of NOD/SCID mice was significantly lower than C57BL/6 mice at 48 h post-CPR (55.88% vs. 75.80%; $\chi^2 = 5.688$; $P < 0.01$).

Giemsa staining of bronchoalveolar lavage fluid after cardiopulmonary resuscitation

The ratio of macrophages/total cells peaked at 2 h postresuscitation in C57BL/6 mice, and the ratio returned to baseline levels at 48 h after CPR. The ratio of neutrophils to total cell numbers continued to significantly increase.

Compared to C57BL/6 mice, the ratio of macrophages/total cells peaked at 12 h and was significantly higher in NOD/SCID mice (31.17 ± 4.13 vs. 49.69 ± 2.43, $t = 14.46$, $P = 0.001$). After 24 h, the results showed a downward trend. Furthermore, a large number of macrophages were disintegrated in the BALF.

The ratio of neutrophils/total cells dramatically increased and remained elevated in C57BL/6 mice for 48 h [Figure 1]. The ratio of neutrophils to total cell numbers also significantly increased in NOD/SCID mice, but the increase was much smaller than in the C57BL/6 mice (9.12 ± 0.75 vs. 22.73 ± 1.34, $t = 18.92$, $P = 0.001$).

The ratio of alveolar epithelial cells/total cells also increased at all time points after ROSC in C57BL/6 mice [Figure 1]. The ratio of alveolar epithelial cells to total cell numbers also increased in NOD/SCID mice, but the increase was much smaller than in the C57BL/6 mice, especially at 24 and 28 h after ROSC (24 h after CPR: 42.53 ± 5.91 vs. 60.79 ± 5.30, $t = 10.88$, $P = 0.001$ and 48 h after CPR: 45.73 ± 4.41 vs. 71.55 ± 6.47, $t = 15.91$, $P = 0.001$).

Phenotypic analysis of macrophages in lung interstitial tissue with flow cytometry during 48 h after cardiopulmonary resuscitation

In the C57BL/6 mice, the number of migrating macrophages ($CD11b^+$ $CD11c^-$) showed a gradual and sustained increase (25.75 ± 1.02 vs. 59.08 ± 4.24, $t = 29.07$, $P = 0.001$) for 48 h after CPR. Compared to C57BL/6 mice, the number of migrating macrophages derived from the bone marrow in the NOD/SCID mice peaked at 12 h after CPR and then gradually decreased at 48 h [Figure 2].

Macrophage debris ($CD11b^-$ $CD11c^-$) and macrophages *in situ* in the lung interstitium ($CD11b^-$ $CD11c^+$) increased gradually in the NOD/SCID mice (macrophages *in situ* 4.00 ± 0.31 vs. 29.25 ± 2.72, $t = 29.01$, $P = 0.001$) after CPR, but the increase was short lived (up to 12 h) and then began to decline in the C57BL/6 mice [Figure 2].

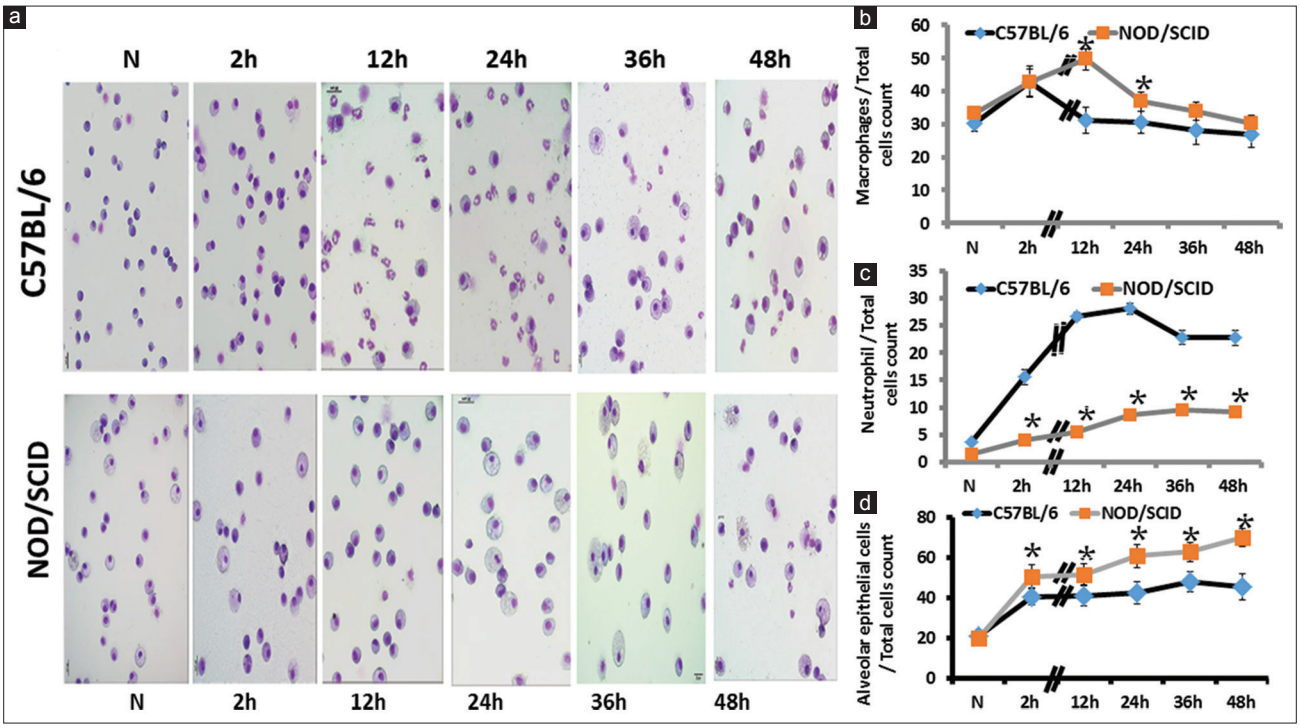

Figure 1: Rare neutrophils and macrophages disintegrate in BALF, and a large number of alveolar epithelial cells were shed at 48 h after resuscitation in NOD/SCID mice. (a) Representative pictures of Giemsa staining of BALF during the 48 h following CPR in C57BL/6 mice and NOD/SCID mice. (b–d) Quantification of the ratio of macrophages, neutrophils, and alveolar epithelial cells to total cells counts by Giemsa staining in BALF ($n = 4$ mice each group). At least 200 cells were examined in each slice, and at least four slices were examined in each mouse. The data are shown as the mean ± standard deviation. *$P < 0.01$ compared to the corresponding C57BL/6 group at the same time after CPR. BALF: Bronchoalveolar lavage fluid; NOD/SCID: Nonobese diabetic/severe combined immunodeficient; CPR: Cardiopulmonary resuscitation.

Table 1: ROSC and survival rate during 48 h after CPR in C57BL/6 and NOD/SCID mice

Mice	Total number	Control groups	ROSC	ROSC rate (%)	2 h post-CPR	12 h post-CPR	24 h post-CPR	48 h post-CPR
C57BL/6	100	8	62	67.39	11 (10)	12 (5)	12 (0)	12 (0)
NOD/SCID	100	8	68	73.91	8 (18)	10 (8)	10 (4)	10 (0)

The number of mice that survived is indicated outside the parentheses, and the number in the parentheses indicates the number of dead mice. ROSC: Return of spontaneous circulation; CPR: Cardiopulmonary resuscitation; NOD: Nonobese diabetic; SCID: Severe combined immunodeficient.

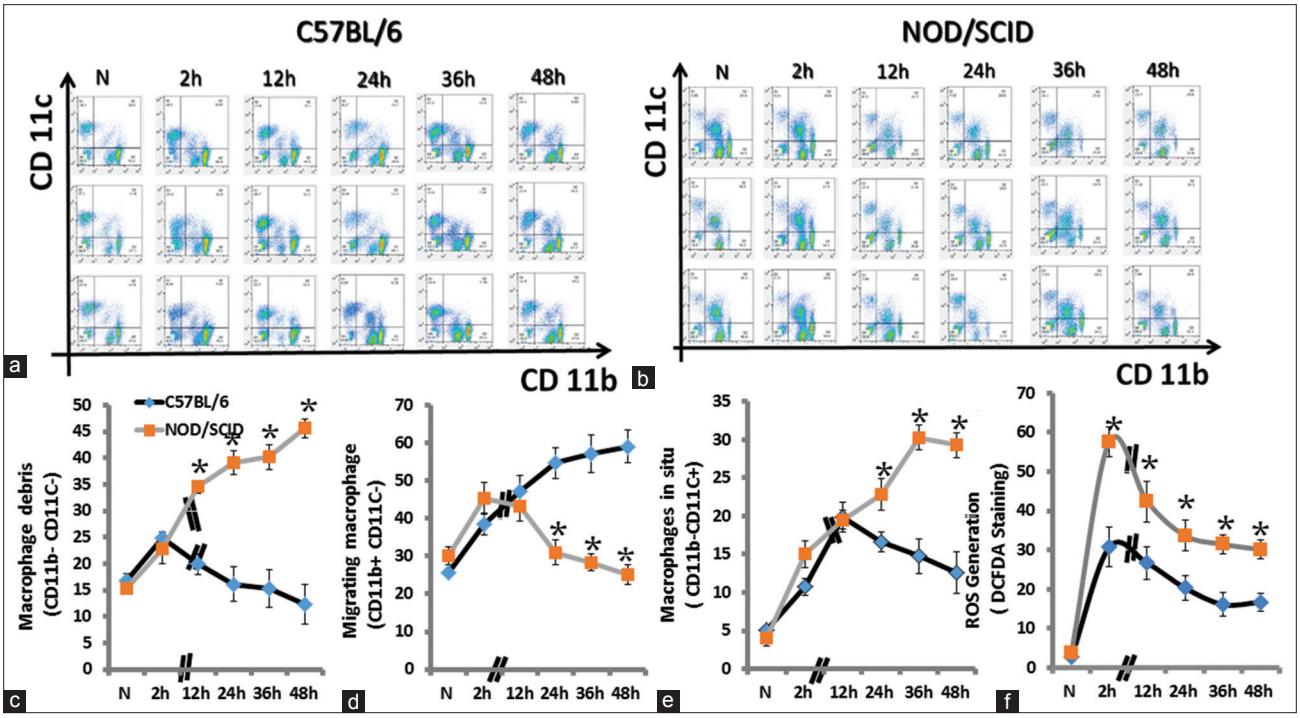

Figure 2: In the C57BL/6 mice, the number of migrating macrophages ($CD11b^+$ $CD11c^-$) showed a gradual increase during the 48 h following CPR. In NOD/SCID mice, macrophages proliferated *in situ* ($CD11b^-$ $CD11c^+$) in the early postresuscitation stages and then disintegrated ($CD11b^-$ $CD11c^-$) extensively after 24 h post-CPR. (a) Representative pictures showing phenotypic analysis of macrophages in lung interstitial tissue with flow cytometry in C57BL/6 mice during the 48 h after CPR. (b) Representative pictures showing phenotypic analysis of macrophages in lung interstitial tissue with flow cytometry in NOD/SCID mice during the 48 h after CPR. (c–f) Spatial characterization of phenotypic analysis of macrophages in lung interstitial tissue as analyzed by flow cytometry ($n = 4$ each group). The data are shown as the mean ± standard deviation. *$P < 0.01$ compared to the corresponding C57BL/6 group at the same time after CPR. NOD/SCID: Nonobese diabetic/severe combined immunodeficient; CPR: Cardiopulmonary resuscitation.

Mitochondria morphological changes in pulmonary functions for 48 h after cardiopulmonary resuscitation

Representative TEM images of mitochondria in C57BL/6 and NOD/SCID mice are shown in Figure 3. The mitochondria were intact, the cristae were smooth and clear, and the stroma was homogeneous in the control groups of C57BL/6 mice and NOD/SCID mice. In C57BL/6 mice, mitochondrial swelling, cristae rupture, and vacuole formation were observed at 2 h after resuscitation. The mitochondria were swollen, the density of the matrix was reduced, and the ridge was rough at 12 h after resuscitation. At 24 h post-CPR, autophagosomes and autolysosomes were present. At 48 h after CPR, autolysosomes were observed, and mitochondrial damage was better than it was before in the C57BL/6 mice.

No differences were observed in the morphology, size, and structure of mitochondria from C57BL/6 and NOD/SCID mice before CPR. In the NOD/SCID mice, mitochondria were condensed at 2 h post-CPR. At 12 h post-CPR, there was mitochondrial swelling, broken cristae, decreased matrix density, and mitochondrial vacuolation. The number of mitochondria with injury (less than Score 2) was significantly higher in NOD/SCID mice than that in C57BL/6 mice. At 24 h after CPR, a large number of mitochondria were destroyed and autophagosomes were rare. At 48 h after CPR, autophagosomes and extensive autolysosomes were present, and the number of damaged mitochondria was higher in the NOD/SCID mice than in the C57BL/6 mice [Figure 4].

Semiquantitative evaluation (Flameng index) of lung tissues revealed that the mitochondrial injury was significantly higher in NOD/SCID mice than in C57BL/6 mice during the 48 h after CPR (at 12, 24, and 48 h after CPR) [Table 2].

Protein expression and activation of ULK1 during the 48 h after cardiopulmonary resuscitation

ULK1, which is a key protein for mitochondrial autophagy initiation, is regulated by the adenosine 5'-monophosphate-activated protein kinase (AMPK) and mammalian target of rapamycin (mTOR2) signaling pathway. It is phosphorylated by AMPK at Ser^{327} and by mTOR at Ser^{757}. In addition, AMPK promotes autophagy in mitochondria, while mTOR2 inhibits autophagy.[24-31]

Compared to the control group, the expression of ULK1 in C57BL/6 mice significantly increased at 2 h and reached its highest level 24 h after CPR. It is noteworthy that autophagy signals were triggered later in NOD/SCID mice than in the C57BL/6 mice.

Specifically, compared to C57BL/6 mice, phos-ULK1 (Ser^{327}) expression was significantly lower at 2 h and 12 h after CPR (2 h after CPR: 1.88 ± 0.36 vs. 1.12 ± 0.11, $t = -1.36$, $P < 0.01$ and 12 h after CPR: 1.52 ± 0.16 vs. 1.05 ± 0.12, $t = -0.33$, $P < 0.01$),

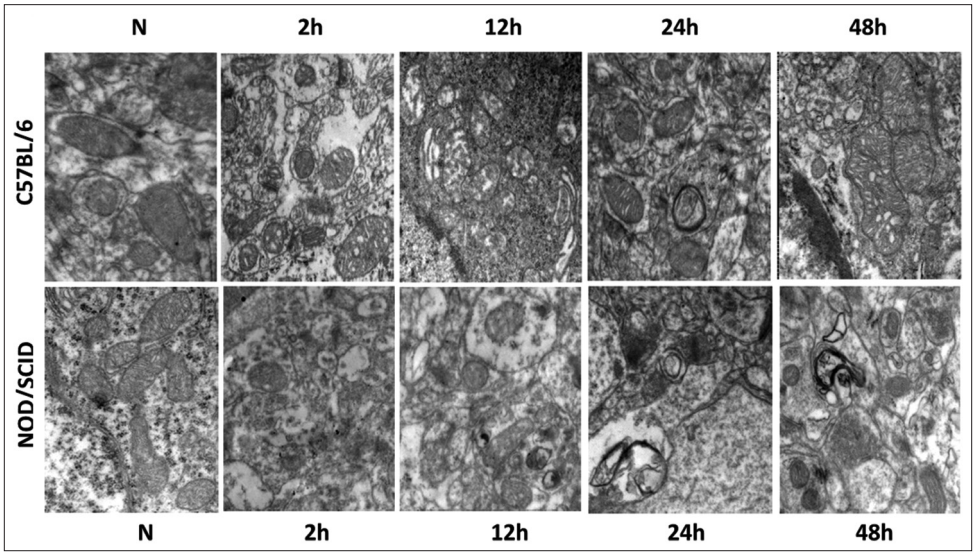

Figure 3: Representative pictures showing mitochondrial damage in lung tissue for 48 h after CPR in C57BL/6 mice and NOD/SCID mice with a transmission electron microscope (×16,000). In NOD/SCID mice, mitochondria were condensed at 2 h post-CPR. At 12 h post-CPR, there was mitochondrial swelling, broken cristae, decreased matrix density, and mitochondrial vacuolation. At 24 h after CPR, a large number of mitochondria were destroyed, and autophagosomes were rare. At 48 h after CPR, autophagosomes and extensive autolysosomes were present, and the number of damaged mitochondria was higher in the NOD/SCID mice than in the C57BL/6 mice. NOD/SCID: Nonobese diabetic/severe combined immunodeficient; CPR: Cardiopulmonary resuscitation.

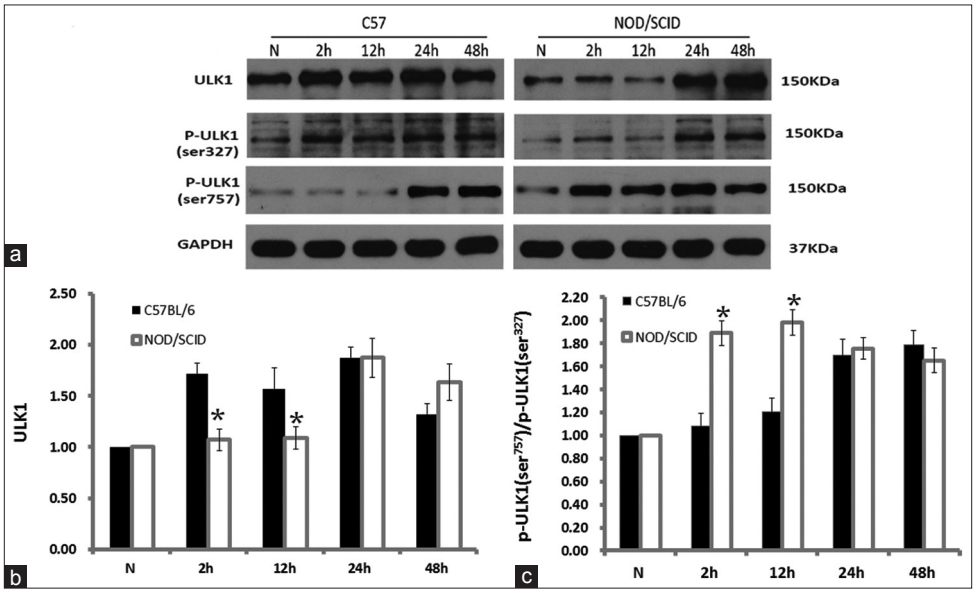

Figure 4: Compared with the C57BL/6 control group (N), expression of ULK1 in C57BL/6 mice significantly increased at 2 h and reached its highest level at 24 h after CPR. The mitochondrial autophagy signal was started much later in NOD/SCID mice. Compared to C57BL/6 mice, phos-ULK1 (Ser^{327}) expression was significantly lower at 2 h and 12 h after CPR ($P < 0.01$) in NOD/SCID mice, whereas phos-ULK1 (Ser^{757}) expression was significantly higher at 2 h and 12 h after CPR ($P < 0.01$) in NOD/SCID mice. (a) Representative Western blots of ULK1, p-ULK1 (ser^{327}), and p-ULK1 (ser^{757}). (b and c) Quantification of Western blot data ($n = 4$ mice each group). The data are shown as the mean ± standard deviation. *$P < 0.01$ compared to corresponding C57BL/6 group at the same time after CPR. NOD/SCID: Nonobese diabetic/severe combined immunodeficient; CPR: Cardiopulmonary resuscitation.

Table 2: Semiquantitative evaluation (Flameng index) of mitochondrial injury in lung tissues for 48 h after CPR

Mice	Control group	2 h post-CPR group	12 h post-CPR group	24 h post-CPR group	48 h post-CPR group
C57BL/6	0 ± 0.001	2.97 ± 0.16	2.54 ± 0.22	1.73 ± 0.12	1.65 ± 0.38
NOD/SCID	0.12 ± 0.01	3.23 ± 0.36	3.05 ± 0.20*	3.52 ± 0.27†	3.72 ± 0.23†
t	6.57	0.88	1.92	7.02	6.49
P	0.001	0.417	0.049	<0.01	0.001

*P<0.05, †P<0.01. n = 6/group. CPR: Cardiopulmonary resuscitation; NOD: Nonobese diabetic; SCID: Severe combined immunodeficient.

whereas phos-ULK1 (Ser^{757}) expression was significantly higher at 2 h and 12 h after CPR in NOD/SCID mice (2 h after CPR: 1.28 ± 0.12 vs. 1.69 ± 0.14, $t = 1.7$, $P < 0.01$ and 12 h after CPR: 1.33 ± 0.10 vs. 1.94 ± 0.13, $t = 2.75$, $P < 0.01$).

These data indicate that the pro-autophagy signals were triggered later in NOD/SCID mice as compared to C57BL/6 mice, and the anti-autophagy signals were triggered earlier in NOD/SCID mice as compared to C57BL/6 mice [Figure 4a].

Protein expression and activation of beclin-1 during 48 h after resuscitation

Beclin-1 is an important regulator of mitochondrial autophagy that is located downstream of the ULK1 promoter.[31,32] AMPK phosphorylates beclin-1 to promote mitochondrial autophagy [Figure 5a, 5c].

Compared to the control group, phos-Beclin-1 (Ser^{93}) increased gradually in both the C57BL/6 and NOD/SCID groups during the 48 h after resuscitation. No significant difference was observed in phos-Beclin-1 (Ser^{93}) between the C57BL/6 and NOD/SCID groups ($P > 0.05$).

Detection of the mitochondrial autophagic flux for 48 h after cardiopulmonary resuscitation

We detected autophagic flux by Western blotting analysis including the ratio of LC3II/LC3I and LC3II/p62. The elevation of LC3II/LC3I represents the initiation of autophagy. LC3 II rises and p62 decreases simultaneously, indicating that the autophagy can be clear up; if LC3II and p62 rise, indicating that autophagy starts normally, but the downstream does not pass and phagosomes and lysosomes cannot fuse.

A Western blot revealed no difference in the expression of LC3B-II in C57BL/6 and NOD/SCID mice at baseline. Compared to the control groups, LC3B-II protein expression in lung tissues was significantly elevated at 12 h after CPR in C57BL/6 mice, and in NOD/SCID mice, and it further increased at 24 h and 48 h after CPR. At 12 and 24 h post-CPR, LC3B-II protein expression in lung tissues from NOD/SCID mice was lower than in C57BL/6 mice (12 h after CPR: 1.20 ± 0.21 vs. 2.42 ± 0.12, $t = 4.24$, $P = 0.001$ and 24 h after CPR: 1.04 ± 0.19 vs. 3.45 ± 0.11, $t = 8.80$, $P = 0.001$). Moreover, meanwhile, p62 protein expression was significantly elevated at 2 and 12 h after CPR in C57BL/6 mice, and in NOD/SCID mice, and it decreased dramatically at 24 h and 48 h after CPR [Figure 5b, 5d]. Therefore, the mitochondrial autophagy pathway including the initial of autophagy and the formation of phagolysosomes were activated in both groups after CPR. However, mitochondrial autophagy was not fully activated in NOD/SCID mice.

Expression of Bax, Smac/Diablo, and cytochrome c during 48 h after cardiopulmonary resuscitation

Smac/Diablo, which is a 21-kDa mammalian protein released from mitochondria, competitively binds to inhibitor of apoptosis proteins (IAPs) and suppresses the inhibitory role of IAPs on the caspases. Thus, Smac/Diablo could promote apoptosis.

Cyto c is found in the inner membrane of the mitochondrion and is an essential component of the electron transport chain. During mitochondrial stress, cyto c is released from the mitochondrion and interacts with procaspase-9/Apaf 1. This complex activates caspase-9, which leads to caspase-3 activation and apoptosis.

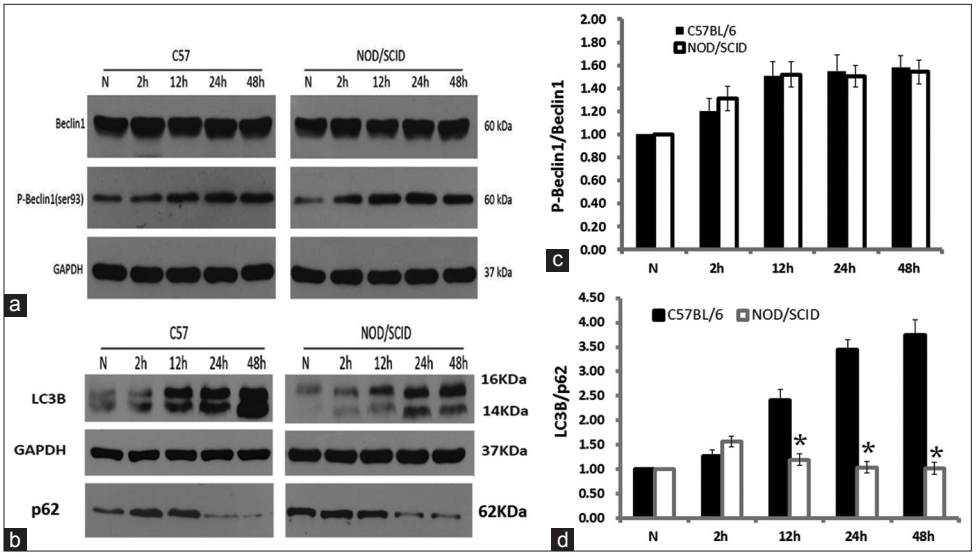

Figure 5: There was no significant difference in phos-Beclin-1 (Ser^{93}) between C57BL/6 and NOD/SCID mice ($P > 0.05$). At 12, 24, and 48 h post-CPR, the ratio of LC3B/p62 protein expression in lung tissues from NOD/SCID mice was much lower than in C57BL/6 mice ($P < 0.01$). (a) Representative Western blots of Beclin1 and its phosphorylation. (b) Representative Western blots of the ratio of LC3B/p62 protein expression. (c and d) Quantification of Western blot data ($n = 4$ mice each group). The data are shown as the mean ± standard deviation. *$P < 0.01$ compared with the corresponding C57BL/6 group at the same time after CPR. NOD/SCID: Nonobese diabetic/severe combined immunodeficient; CPR: Cardiopulmonary resuscitation.

Bax, which is an important pro-apoptotic factor, interacts with Bcl-2 to regulate apoptosis. A Western blot revealed that BAX protein expression peaked at 2 h after CPR and gradually decreased at 24 and 48 h after CPR in C57BL/6 mice. Bax protein levels gradually increased for 48 h after CPR in NOD/SCID mice [Figure 6]. In NOD/SCID mice, cyto c expression increased at 12, 24, and 48 h after CPR, peaking at 24 h post-CPR. The difference in cyto c expression in the two groups of mice was significant (1.10 ± 0.10 vs. 1.61 ± 0.19, $t = 1.89$, $P < 0.01$). Smac/Diablo expression increased in the lung tissues from NOD/SCID mice at 24 and 48 h after CPR but not in the C57BL mice ($P < 0.01$).

Activation of the NLRP3 inflammasome and caspase-1 after cardiopulmonary resuscitation

The expression of the NLRP3 inflammasome increased modestly in the C57 mice, but the increase was higher in the NOD/SCID mice than in the C57BL/6 mice, especially at 12, 24, and 48 h after CPR (48 h after CPR: 1.46 ± 0.13 vs. 2.97 ± 0.19, $t = 5.34$, $P = 0.001$). The expression of caspase-1-20 generally followed the same pattern as the NLRP3 inflammasome [Figure 7].

After CPR, the NLRP3 inflammasome and caspase-1 were continuously activated in NOD/SCID mice starting at 12 h post-CPR, leading to caspase-1-dependent cell pyroptosis, which is an event that can take place between apoptosis and necrosis. Consistent with these data, the amount of macrophage debris ($CD11b^{-}$ $CD11c^{-}$) and the number of disintegrated macrophages were greater in the BALF at 24 and 48 h after CPR in the NOD/SCID mice than in C57BL/6 mice.

Discussion

In rodent, porcine, and canine cardiac arrest models, respiratory failure occurs soon following CPR and the ROSC. The pulmonary function then recovers in 48–72 h after CPR in healthy animals. In immunocompromised animals, CPR induces a long period of severe respiratory failure with irreversible injury, which significantly decreases survival.[1,33,34] Immunocompromised patients also suffer from a high incidence of systemic inflammatory responses and severe multiorgan dysfunction as well as high mortality after CPR.

In our study, although a higher ROSC rate was observed in NOD/SCID mice, their survival rate was significantly lower than that of C57BL/6 mice over the 48 h post-CPR ($P < 0.05$). These findings are similar to previous findings in animals and humans.[1,33,34]

We show that the lung tissue had a self-healing inflammatory response during the 48 h after CPR in C57BL/6 mice, which manifested as increase in the number of migrating macrophages and neutrophils. This outcome was similar to the response in participants with normal immune function that showed a Th1 inflammatory pattern of granulocyte mobilization from the bone marrow to the peripheral circulation, migration of neutrophils, and recruitment of monocytes to the lung tissue. All these exert anti-inflammatory effects. However, SCID mice showed a Th2 inflammatory pattern in which the macrophages proliferated *in situ* in the early stages of postresuscitation, followed by the disintegration of these macrophages. This disintegration was accompanied by the shedding of a large number of alveolar epithelial cells, which produced extensive injury to organs. Neutrophils are key effectors of the innate immune response. Reduced neutrophil migration to infection sites leads to lethal sepsis.[1,33,34] We have demonstrated a failure of neutrophil migration in SCID mice with poor outcomes after CPR.

In addition, our study demonstrated that the mitochondrial autophagy signaling pathway was initiated in mice with normal immune and immune-deficient mice after

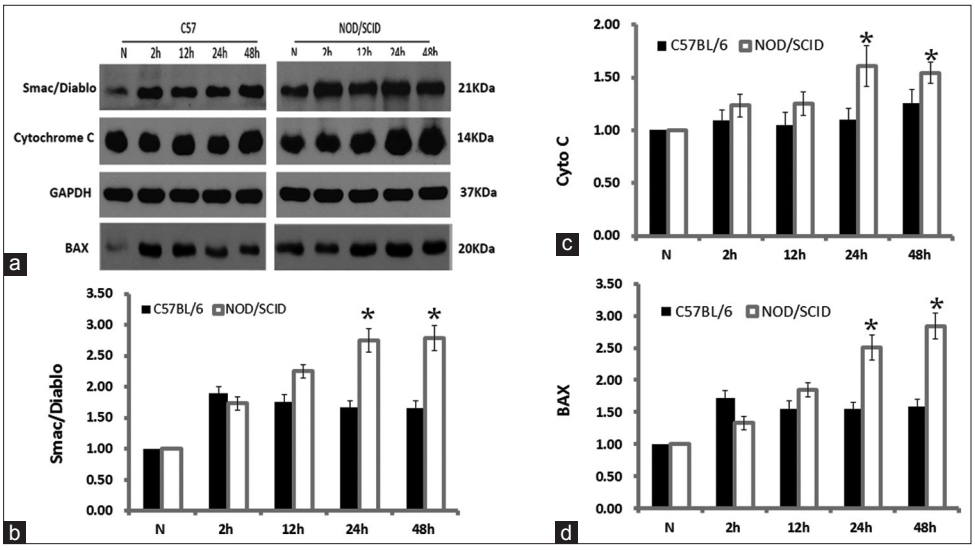

Figure 6: At 24 and 48 h after CPR, the apoptosis proteins released from mitochondria were significantly increased in NOD/SCID mice compared to those in C57BL/6 mice. (a) Representative Western blots of Smac/Diablo, cytochrome c, and Bax. (b-d) Quantification of Western blot data ($n = 4$ mice each group). The data are shown as the mean ± standard deviation. *$P < 0.01$ compared to the corresponding C57BL/6 group at the same time after CPR. NOD/SCID: Nonobese diabetic/severe combined immunodeficient; CPR: Cardiopulmonary resuscitation.

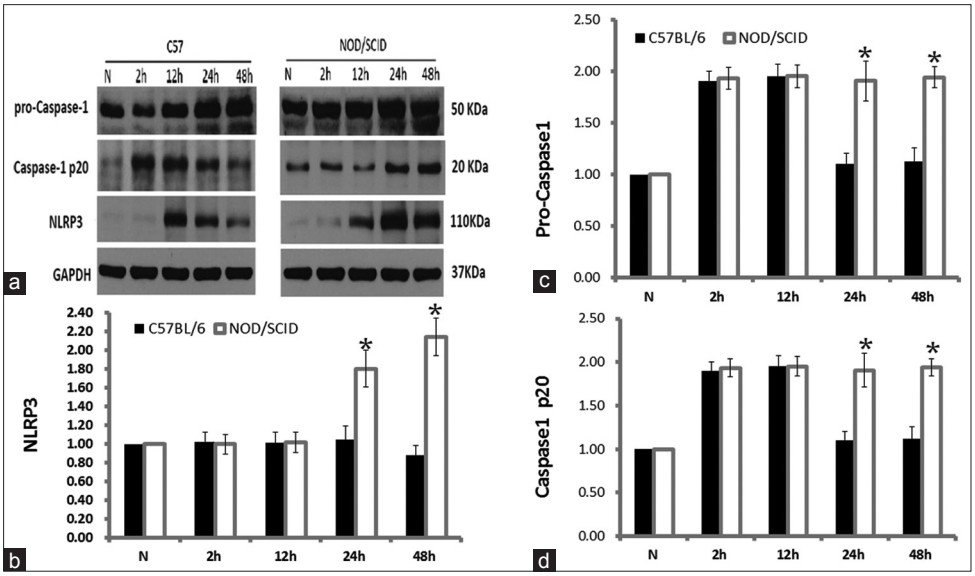

Figure 7: At 24 and 48 h after CPR, NLRP3 inflammasome and caspase-1 p20 protein levels were significantly increased in NOD/SCID mice compared to those in C57BL/6 mice. (a) Representative Western blots of the NLRP3 inflammasome, pro-caspase-1, and caspase-1 p20. (b-d) Quantification of Western blot data ($n = 4$ mice each group). The data are shown as the mean ± standard deviation. *$P < 0.01$ compared to the corresponding C57BL/6 group at the same time after CPR. NOD/SCID: Nonobese diabetic/severe combined immunodeficient; CPR: Cardiopulmonary resuscitation.

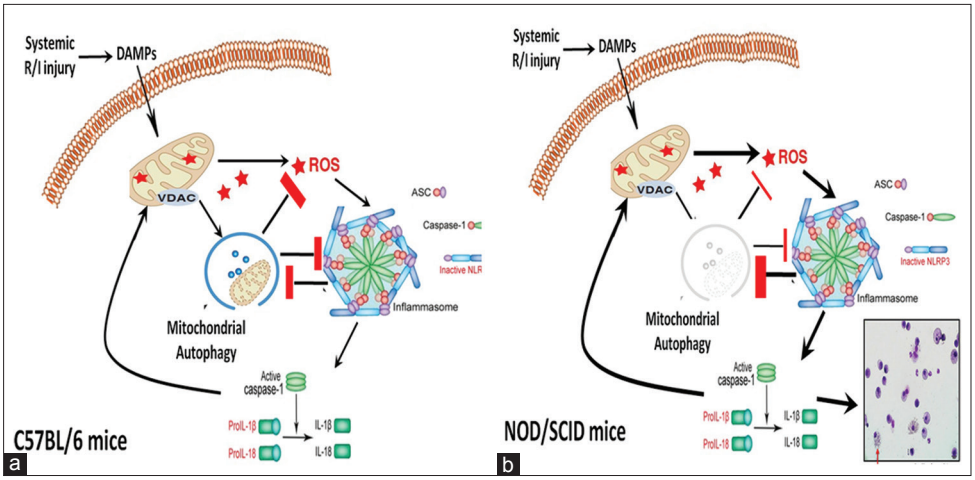

Figure 8: Proposed signaling loop of mitochondrial ROS→NLRP3 inflammasome→caspase-1→mitochondrial ROS during CPR-induced ischemia-reperfusion (I/R) injury. (a) C57BL/6 mice initiated mitochondrial autophagy early and inhibited the expression of the NLRP3 inflammasome in the early stages following cardiopulmonary resuscitation. (b) NOD/SCID mice did not start mitochondrial autophagy properly in the early stages of post-resuscitation. Without mitochondrial autophagy, there appears to be a positive feedback loop among mitochondrial ROS, the NLRP3 inflammasome, and caspase-1, which leads to caspase-1-dependent cell pyroptosis. NOD/SCID: Nonobese diabetic/severe combined immunodeficient; CPR: Cardiopulmonary resuscitation; ROS: Reactive oxygen species; I/R: Ischemia-reperfusion.

CPR. Compared to C57BL/6 mice, the mitochondrial autophagy signal was activated much later in NOD/SCID mice; however, the specific reasons are not clear.[35-40] We further explored the reasons for delayed initiation of mitochondrial autophagy in the early stages of I/R injury in immunocompromised mice. Competitive phosphorylation of ULK1 is critical for the regulation of mitochondrial autophagy. AMPK directly phosphorylates ULK1 at Ser^{327} and Ser^{777} to induce autophagy in mitochondria with minor injuries. mTOR is a negative regulator of mitochondrial autophagy. Previous evidence suggests that stimulation with insulin-like growth factor leads to mTOR activation mediated by P13K/AKT signals to inhibit autophagy. Specifically, enhanced activity of mTOR phosphorylates ULK1 at Ser^{757} to block the interaction between ULK1 and AMPK in energy-sufficient conditions.[24-31] Our results showed that, compared to C57BL/6 mice, phos-ULK1 (Ser^{327}), which promotes autophagy, had significantly lower expression and phos-ULK1 (Ser^{757}), which inhibits autophagy, had significantly higher expression in NOD/SCID mice in the early stage of postresuscitation. Obviously, beclin-1, which is another important regulator of mitochondrial autophagy, was not as effective as we expected.

Our study demonstrated that, at the early stages of postresuscitation, C57BL/6 mice initiated mitochondrial autophagy and inhibited the overexpression of the NLRP3 inflammasome. Therefore, it reduced the excessive activation of caspase-1 in the late stages of postresuscitation. Thus, the immune-normal individuals showed a transient self-repair inflammation response in PCAS.

The NOD/SCID mice did not properly initiate mitochondrial autophagy in the early stages of postresuscitation, which resulted in mitochondrial ROS → NLRP3 inflammasome → caspase-1 → mitochondrial ROS, and this signal loop continued to amplify the stress signal, continued to the expand inflammatory response, and led to caspase-1-dependent cell pyroptosis.[41-54] Specifically, the NLRP3 inflammasome continued to express caspase-1 and continued to activate the late stage of postresuscitation in NOD/SCID mice [Figure 8]. This result may partially explain why the survival rate of immunodeficient mice was significantly lower than that of mice with intact immune function in the 48 h following CPR.

In conclusion, our research confirmed that (1) there is a negative regulatory relationship between the NLRP3 inflammasome and mitochondrial autophagy. For individuals with normal immune function, this relationship is the core part of PCAS that exhibits reversible self-repairable inflammatory responses, and (2) we did not thoroughly explain why NOD/SCID mice did not initiate mitochondrial autophagy properly in the early stages of postresuscitation. That was a limitation of this study.

Part of the reason for that limitation is that we are using NOD/SCID mice without using single gene knockout mice in a CPR model. The original intention is that we encountered immunodeficient patients, such as individuals with long-term use of glucocorticoids, organ transplant patients using anti-rejection drugs, or cancer patients receiving chemotherapy or radiotherapy, and immunodeficiency itself does not occur due to a single genetic defect leading to cellular immunodeficiency or humoral immunodeficiency.

Supplementary information is linked to the online version of the paper on the Chinese Medical Journal website.

Financial support and sponsorship

This work was supported by grants from the National Natural Science Foundation of China (No. 81372020), the Foundation of Young Talent Physician Training Project in Wuhan City (No. 2014ZX0001) and Guiding Foundation of Renmin Hospital of Wuhan University (No. RMYD 2018Z15).

Conflicts of interest

There are no conflicts of interest.

References

1. Callaway CW, Donnino MW, Fink EL, Geocadin RG, Golan E, Kern KB, *et al.* Part 8: Post-cardiac arrest care: 2015 American Heart Association guidelines update for cardiopulmonary resuscitation and emergency cardiovascular care. Circulation 2015;132:S465-82. doi: 10.1161/CIR.0000000000000262.
2. Parzych KR, Klionsky DJ. An overview of autophagy: Morphology, mechanism, and regulation. Antioxid Redox Signal 2014;20:460-73. doi: 10.1089/ars.2013.5371.
3. Lu J, Mitra S, Wang X, Khaidakov M, Mehta JL. Oxidative stress and lectin-like ox-LDL-receptor LOX-1 in atherogenesis and tumorigenesis. Antioxid Redox Signal 2011;15:2301-33. doi: 10.1089/ars.2010.3792.
4. Wirawan E, Vanden Berghe T, Lippens S, Agostinis P, Vandenabeele P. Autophagy: For better or for worse. Cell Res 2012;22:43-61. doi: 10.1038/cr.2011.152.
5. Jiang P, Mizushima N. Autophagy and human diseases. Cell Res 2014;24:69-79. doi: 10.1038/cr.2013.161.
6. Green DR, Galluzzi L, Kroemer G. Cell biology. Metabolic control of cell death. Science 2014;345:1250256. doi: 10.1126/science.1250256.
7. Lee J, Giordano S, Zhang J. Autophagy, mitochondria and oxidative stress: Cross-talk and redox signalling. Biochem J 2012;441:523-40. doi: 10.1042/BJ20111451.
8. Green DR, Levine B. To be or not to be? How selective autophagy and cell death govern cell fate. Cell 2014;157:65-75. doi: 10.1016/j.cell.2014.02.049.
9. Eltzschig HK, Eckle T. Ischemia and reperfusion – From mechanism to translation. Nat Med 2011;17:1391-401. doi: 10.1038/nm.2507.
10. Khan MM, Yang WL, Wang P. Endoplasmic reticulum stress in sepsis. Shock 2015;44:294-304. doi: 10.1097/SHK.0000000000000425.
11. Haugaa H, Gómez H, Maberry DR, Holder A, Ogundele O, Quintero AM, *et al.* Effects of inhalation of low-dose nitrite or carbon monoxide on post-reperfusion mitochondrial function and tissue injury in hemorrhagic shock swine. Crit Care 2015;19:184. doi: 10.1186/s13054-015-0903-z.
12. Cui D, Shang H, Zhang X, Jiang W, Jia X. Cardiac arrest triggers hippocampal neuronal death through autophagic and apoptotic pathways. Sci Rep 2016;6:27642. doi: 10.1038/srep27642.
13. Fang B, Li XQ, Bao NR, Tan WF, Chen FS, Pi XL, *et al.* Role of autophagy in the bimodal stage after spinal cord ischemia reperfusion injury in rats. Neuroscience 2016;328:107-16. doi: 10.1016/j.neuroscience.2016.04.019.
14. Dezfulian C, Shiva S, Alekseyenko A, Pendyal A, Beiser DG, Munasinghe JP, *et al.* Nitrite therapy after cardiac arrest reduces reactive oxygen species generation, improves cardiac and neurological function, and enhances survival via reversible inhibition of mitochondrial complex I. Circulation 2009;120:897-905. doi: 10.1161/CIRCULATIONAHA.109.853267.
15. Kamga Pride C, Mo L, Quesnelle K, Dagda RK, Murillo D, Geary L, *et al.* Nitrite activates protein kinase A in normoxia to mediate mitochondrial fusion and tolerance to ischaemia/reperfusion. Cardiovasc Res 2014;101:57-68. doi: 10.1093/cvr/cvt224.
16. Uchiyama Y, Koike M, Shibata M. Autophagic neuron death in neonatal brain ischemia/hypoxia. Autophagy 2008;4:404-8. doi: 10.4161/auto.5598.
17. Gump JM, Thorburn A. Autophagy and apoptosis: What is the connection? Trends Cell Biol 2011;21:387-92. doi: 10.1016/j.tcb.2011.03.007.
18. Lu J, Wang X, Wang W, Muniyappa H, Deshmukh A, Hu C, *et al.* Abrogation of lectin-like oxidized LDL receptor-1 attenuates acute myocardial ischemia-induced renal dysfunction by modulating systemic and local inflammation. Kidney Int 2012;82:436-44. doi: 10.1038/ki.2012.186.
19. Shirakabe A, Ikeda Y, Sciarretta S, Zablocki DK, Sadoshima J. Aging and autophagy in the heart. Circ Res 2016;118:1563-76. doi: 10.1161/CIRCRESAHA.116.307474.
20. Vermaelen K, Pauwels R. Accurate and simple discrimination of mouse pulmonary dendritic cell and macrophage populations by flow cytometry: Methodology and new insights. Cytometry A 2004;61:170-77. doi: 10.1002/cyto.a.20064.
21. Janssen WJ, Barthel L, Muldrow A, Oberley-Deegan RE, Kearns MT, Jakubzick C, *et al.* Fas determines differential fates of resident and recruited macrophages during resolution of acute lung injury. Am J Respir Crit Care Med 2011;184:547-60. doi: 10.1164/rccm.201011-1891OC.

22. Ji WJ, Ma YQ, Zhou X, Zhang YD, Lu RY, Sun HY, *et al.* Temporal and spatial characterization of mononuclear phagocytes in circulating, lung alveolar and interstitial compartments in a mouse model of bleomycin-induced pulmonary injury. J Immunol Methods 2014;403:7-16. doi: 10.1016/j.jim.2013.11.012.
23. Ding Z, Liu S, Wang X, Dai Y, Khaidakov M, Deng X, *et al.* LOX-1, mtDNA damage, and NLRP3 inflammasome activation in macrophages: Implications in atherogenesis. Cardiovasc Res 2014;103:619-28. doi: 10.1093/cvr/cvu114.
24. Kim J, Kundu M, Viollet B, Guan KL. AMPK and mTOR regulate autophagy through direct phosphorylation of ulk1. Nat Cell Biol 2011;13:132-41. doi: 10.1038/ncb2152.
25. Egan DF, Shackelford DB, Mihaylova MM, Gelino S, Kohnz RA, Mair W, *et al.* Phosphorylation of ULK1 (hATG1) by AMP-activated protein kinase connects energy sensing to mitophagy. Science 2011;331:456-61. doi: 10.1126/science.1196371.
26. Gallagher LE, Williamson LE, Chan EY. Advances in autophagy regulatory mechanisms. Cells 2016;5. pii: E24. doi: 10.3390/cells5020024.
27. Park JM, Jung CH, Seo M, Otto NM, Grunwald D, Kim KH, *et al.* The ULK1 complex mediates MTORC1 signaling to the autophagy initiation machinery via binding and phosphorylating ATG14. Autophagy 2016;12:547-64. doi: 10.1080/15548627.2016.1140293.
28. Lin SY, Li TY, Liu Q, Zhang C, Li X, Chen Y, *et al.* GSK3-TIP60-ULK1 signaling pathway links growth factor deprivation to autophagy. Science 2012;336:477-81. doi: 10.1126/science.1217032.
29. Rebsamen M, Pochini L, Stasyk T, de Araújo ME, Galluccio M, Kandasamy RK, *et al.* SLC38A9 is a component of the lysosomal amino acid sensing machinery that controls mTORC1. Nature 2015;519:477-81. doi: 10.1038/nature14107.
30. Tian W, Li W, Chen Y, Yan Z, Huang X, Zhuang H, *et al.* Phosphorylation of ULK1 by AMPK regulates translocation of ULK1 to mitochondria and mitophagy. FEBS Lett 2015;589:1847-54. doi: 10.1016/j.febslet.2015.05.020.
31. Laplante M, Sabatini DM. MTOR signaling in growth control and disease. Cell 2012;149:274-93. doi: 10.1016/j.cell.2012.03.017.
32. Lindqvist LM, Heinlein M, Huang DC, Vaux DL. Prosurvival Bcl-2 family members affect autophagy only indirectly, by inhibiting Bax and Bak. Proc Natl Acad Sci U S A 2014;111:8512-7. doi: 10.1073/pnas.1406425111.
33. Chiswick EL, Mella JR, Bernardo J, Remick DG. Acute-phase deaths from murine polymicrobial sepsis are characterized by innate immune suppression rather than exhaustion. J Immunol 2015;195:3793-802. doi: 10.4049/jimmunol.1500874.
34. Asmussen A, Fink K, Busch HJ, Helbing T, Bourgeois N, Bode C, *et al.* Inflammasome and toll-like receptor signaling in human monocytes after successful cardiopulmonary resuscitation. Crit Care 2016;20:170. doi: 10.1186/s13054-016-1340-3.
35. Kuballa P, Nolte WM, Castoreno AB, Xavier RJ. Autophagy and the immune system. Annu Rev Immunol 2012;30:611-46. doi: 10.1146/annurev-immunol-020711-074948.
36. Puleston DJ, Simon AK. Autophagy in the immune system. Immunology 2014;141:1-8. doi: 10.1111/imm.12165.
37. Deretic V, Kimura T, Timmins G, Moseley P, Chauhan S, Mandell M, *et al.* Immunologic manifestations of autophagy. J Clin Invest 2015;125:75-84. doi: 10.1172/JCI73945.
38. Tang D, Kang R, Coyne CB, Zeh HJ, Lotze MT. PAMPs and DAMPs: Signal 0s that spur autophagy and immunity. Immunol Rev 2012;249:158-75. doi: 10.1111/j.1600-065X.2012.01146.x.
39. Willinger T, Flavell RA. Canonical autophagy dependent on the class III phosphoinositide-3 kinase vps34 is required for naive T-cell homeostasis. Proc Natl Acad Sci U S A 2012;109:8670-5. doi: 10.1073/pnas.1205305109.
40. Weinberg SE, Sena LA, Chandel NS. Mitochondria in the regulation of innate and adaptive immunity. Immunity 2015;42:406-17. doi: 10.1016/j.immuni.2015.02.002.
41. Netea-Maier RT, Plantinga TS, van de Veerdonk FL, Smit JW, Netea MG. Modulation of inflammation by autophagy: Consequences for human disease. Autophagy 2016;12:245-60. doi: 10.1080/15548627.2015.1071759.
42. Suzuki SW, Yamamoto H, Oikawa Y, Kondo-Kakuta C, Kimura Y, Hirano H, *et al.* Atg13 HORMA domain recruits atg9 vesicles during autophagosome formation. Proc Natl Acad Sci U S A 2015;112:3350-5. doi: 10.1073/pnas.1421092112.
43. Moon JS, Lee S, Park MA, Siempos II, Haslip M, Lee PJ, *et al.* UCP2-induced fatty acid synthase promotes NLRP3 inflammasome activation during sepsis. J Clin Invest 2015;125:665-80. doi: 10.1172/JCI78253.
44. Saitoh T, Fujita N, Jang MH, Uematsu S, Yang BG, Satoh T, *et al.* Loss of the autophagy protein Atg16L1 enhances endotoxin-induced IL-1beta production. Nature 2008;456:264-8. doi: 10.1038/nature07383.
45. Sorbara MT, Girardin SE. Mitochondrial ROS fuel the inflammasome. Cell Res 2011;21:558-60. doi: 10.1038/cr.2011.20.
46. Nakahira K, Haspel JA, Rathinam VA, Lee SJ, Dolinay T, Lam HC, *et al.* Autophagy proteins regulate innate immune responses by inhibiting the release of mitochondrial DNA mediated by the NALP3 inflammasome. Nat Immunol 2011;12:222-30. doi: 10.1038/ni.1980.
47. Dupont N, Jiang S, Pilli M, Ornatowski W, Bhattacharya D, Deretic V, *et al.* Autophagy-based unconventional secretory pathway for extracellular delivery of IL-1β. EMBO J 2011;30:4701-11. doi: 10.1038/emboj.2011.398.
48. Jabaut J, Ather JL, Taracanova A, Poynter ME, Ckless K. Mitochondria-targeted drugs enhance nlrp3 inflammasome-dependent IL-1β secretion in association with alterations in cellular redox and energy status. Free Radic Biol Med 2013;60:233-45. doi: 10.1016/j.freeradbiomed.2013.01.025.
49. Yu J, Nagasu H, Murakami T, Hoang H, Broderick L, Hoffman HM, *et al.* Inflammasome activation leads to caspase-1-dependent mitochondrial damage and block of mitophagy. Proc Natl Acad Sci U S A 2014;111:15514-9. doi: 10.1073/pnas.1414859111.
50. Xi H, Zhang Y, Xu Y, Yang WY, Jiang X, Sha X, *et al.* Caspase-1 inflammasome activation mediates homocysteine-induced pyrop-apoptosis in endothelial cells. Circ Res 2016;118:1525-39. doi: 10.1161/CIRCRESAHA.116.308501.
51. Abderrazak A, Syrovets T, Couchie D, El Hadri K, Friguet B, Simmet T, *et al.* NLRP3 inflammasome: From a danger signal sensor to a regulatory node of oxidative stress and inflammatory diseases. Redox Biol 2015;4:296-307. doi: 10.1016/j.redox.2015.01.008.
52. Zhou R, Yazdi AS, Menu P, Tschopp J. A role for mitochondria in NLRP3 inflammasome activation. Nature 2011;469:221-5. doi: 10.1038/nature09663.
53. Bordt EA, Polster BM. NADPH oxidase- and mitochondria-derived reactive oxygen species in proinflammatory microglial activation: A bipartisan affair? Free Radic Biol Med 2014;76:34-46. doi: 10.1016/j.freeradbiomed.2014.07.033.
54. Abais JM, Xia M, Zhang Y, Boini KM, Li PL. Redox regulation of NLRP3 inflammasomes: ROS as trigger or effector? Antioxid Redox Signal 2015;22:1111-29. doi: 10.1089/ars.2014.5994.

严重联合免疫缺陷小鼠心脏骤停心肺复苏后肺组织线粒体自噬与NLRP3炎症小体

摘要

背景：肿瘤、糖尿病、自身免疫系统疾病发病率逐年升高，实体器官移植患者越来越多，这些免疫缺陷个体遭受严重打击时存活率极低。本研究应用严重联合免疫缺陷小鼠建立心搏骤停心肺复苏模型，分析线粒体自噬和NLRP3炎症小体/caspase-1的表达和活化，探讨在系统性缺血再灌注损伤过程中，免疫缺陷个体的线粒体修复和炎症损伤。

方法：应用C57BL/6 小鼠和严重联合免疫缺陷（NOD/SCID）小鼠建立心搏骤停心肺复苏模型。100只雄性C57BL/6小鼠和100只雄性NOD/SCID小鼠随机分组，采用Giemsa染色对各组小鼠心肺复苏前、复苏后2h、12h、24h、36h、48h支气管肺泡灌洗液（BALF）中的肺泡上皮细胞、巨噬细胞和中性粒细胞进行分类计数；采用流式细胞术分析各组小鼠心肺复苏后肺间质组织中巨噬细胞表型；使用透射电镜观察复苏后不同时间点线粒体形态，采用Flameng 分级方法对线粒体损伤进行半定量分析；采用Western blot法检测线粒体自噬流（autophagic flux），以及NLRP3炎症小体/caspase-1表达和激活。

结果：NOD/SCID小鼠肺泡灌洗液中巨噬细胞崩解焦亡，大量肺泡上皮细胞脱落。C57BL/6和NOD /SCID小鼠在心肺复苏后都出现线粒体自噬，但NOD/ SCID小鼠启动得较晚。C57BL/6小鼠肺组织中NLRP3炎症小体/caspase-1表达和激活发生在复苏后早期，并且只持续短暂时间，NOD/SCID小鼠肺组织中NLRP3炎症小体/caspase-1激活持续存在。

结论：在心搏骤停心肺复苏诱导缺血再灌注损伤过程中，线粒体自噬和NLRP3 炎症小体之间存在着负调节关系。免疫功能正常的C57BL/6 小鼠在心肺复苏早期及时启动线粒体自噬，抑制NLRP3 炎症小体持续高表达。NOD / SCID 小鼠在心肺复苏早期没有正确启动线粒体自噬，致使线粒体ROS→NLRP3 炎症小体→Caspase1→线粒体ROS 这一信号环路持续扩增，持续扩大炎症反应，导致Caspase 1 依赖性细胞焦亡。

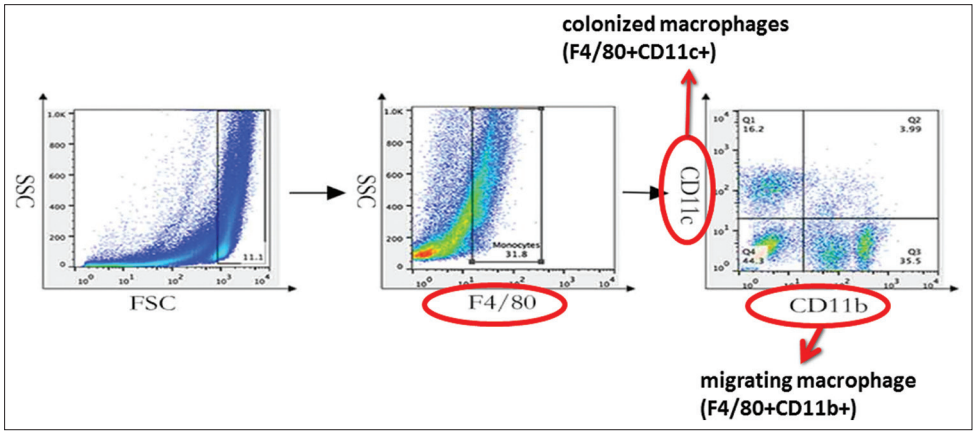

Supplementary Figure 1: The gating strategies for pulmonary interstitial macrophage subsets. Briefly, the cells were labeled with F4/80, CD11c, and CD11b by flow cytometry. The first step involved screening out cell debris. The second step was screening F4/80-positive cells. F4/80 is a surface glycoprotein that is a marker of mature macrophages. In the third step, the percentages of CD11b-positive cells and CD11c-positive cells in the F4/80-positive cell population were determined. CD11b is highly expressed in migrating macrophages, and CD11c is highly expressed in colonized macrophages. FSC: Forward-scattered light; SSC: Side-scattered light.